Optics Near the Snell Angle in a Water-to-Air Change of Medium

H. Suiter,* N. Flacco, Paul Carter, Kelvin Tong, Ryan Ries, and Meir Gershenson*

* Naval Surface Warfare Center Panama City
110 Vernon Ave. Code HS12
Panama City FL 32407

Areté Associates - Los Angeles
9301 Corbin Ave., Suite 2000
Northridge, CA 91324

Abstract - Underwater imaging of the air environment is described with particular attention given to the optical problems of near-horizon viewing. These include severe chromatic aberration from transmission through the seawater wedge, the horizon distortion effect, and anisoplanatism resulting from the change of refractive aberrations in different areas of view. Various optical designs or schemes are presented that correct or relieve the first two optical problems. Strategies to minimize or attempt to view through the varying refraction of the surface are also suggested, and one is investigated.

I. INTRODUCTION

The appearance of the aerial half-sphere from underwater has long been a matter of recreational curiosity and educational interest. It also figures in the survival for fish that rely on jumping or squirting water at in-air prey and the lure-casting accuracy of human anglers [1][2]. This discussion is chiefly about imaging near the horizon or at angles very near the edge of the Snell window (the Snell cone). Imaging under these circumstances is difficult to impossible compared with imaging near the vertical, although the imaging near vertical through disturbed water is itself deemed very difficult. Theoretical calculations have concentrated on the calm-water case [3], but the likelihood of encountering completely calm conditions—even in sheltered bays and rivers—is quite limited.

Imaging near the air-horizon is necessary because so much of what happens that is interesting to sea observers, either immersed or in air, is near the horizon. For example, a huge oil tanker or cruise ship with upper works extending 40 m above the water would occupy angles less than 5 degrees at a distance of only about 460 m (little more than its own length). Lesser objects that one might want to view from a submerged position would likely occupy only the first few degrees from the horizon.

II. THE OPTICAL PROBLEMS

A. Wedge Chromatic Aberration

The Snell cone, because it is tilted at an angle of approximately 48 degrees from the vertical, induces a prism-like spectrum in the incoming ray bundle. It is as if this bundle has traversed a prism with apical angle of 48 degrees. At 510 nm under laboratory pressures and temperatures, light has a modeled index of refraction in seawater of n_{510} = 1.342404 and at 610 nm its index is n_{610} = 1.338877. The spectrum of this virtual wedge of seawater has an angular spread of

$$\theta \cong n_{560}\left[\sin^{-1}\left(\frac{1}{n_{610}}\right)-\sin^{-1}\left(\frac{1}{n_{510}}\right)\right] \quad = \quad 0.226 \text{ degrees,} \tag{1}$$

where n_{560} is the index at 560 nm, the center of the considered spectrum. This subset of the spectrum was chosen following [4], since a visual or a visual-filtered spectrum was the region of greatest interest. Fig. 1 shows the effect of the seawater wedge at the focus of a notional 57.3-mm lens modeled in ZEMAX® [5]. The boxes are plotted in units of μm, and lens focal length is chosen so that 1 mm of movement in the focal plane (1000 μm) is a convenient 1-degree shift in the focal plane. Note that the spectrum is profound at small angle, at a horizon angle of 2 degrees the spectrum length is 3.5degrees. The incidence angles are annotated at left and it is obvious that the length of the spectrum varies little from an incidence angle of 70 degrees (20 degree horizon angle) to 88 degrees (2 degrees horizon angle). Thus, if a lens or corrective mechanism can be found that cures this problem at one angle, it will also be useful over a large field-of-view.

This work is sponsored by the Office of Naval Research, Coastal Geosciences Program.

Report Documentation Page

Form Approved
OMB No. 0704-0188

1. REPORT DATE	2. REPORT TYPE	3. DATES COVERED
SEP 2007		**00-00-2007 to 00-00-2007**

4. TITLE AND SUBTITLE	5a. CONTRACT NUMBER
Optics Near the Snell Angle in a Water-to-Air Change of Medium	5b. GRANT NUMBER
	5c. PROGRAM ELEMENT NUMBER
6. AUTHOR(S)	5d. PROJECT NUMBER
	5e. TASK NUMBER
	5f. WORK UNIT NUMBER
7. PERFORMING ORGANIZATION NAME(S) AND ADDRESS(ES) **Naval Surface Warfare Center Panama City,110 Vernon Ave. Code HS12,Panama City,FL,32407**	8. PERFORMING ORGANIZATION REPORT NUMBER
9. SPONSORING/MONITORING AGENCY NAME(S) AND ADDRESS(ES)	10. SPONSOR/MONITOR'S ACRONYM(S)
	11. SPONSOR/MONITOR'S REPORT NUMBER(S)

12. DISTRIBUTION/AVAILABILITY STATEMENT
Approved for public release; distribution unlimited

13. SUPPLEMENTARY NOTES
See also ADM002047. Presented at the MTS/IEEE Oceans 2007 Conference held in Vancouver, Canada on Sep 29-Oct 4, 2007.

14. ABSTRACT
See Report

15. SUBJECT TERMS

16. SECURITY CLASSIFICATION OF:			17. LIMITATION OF ABSTRACT	18. NUMBER OF PAGES	19a. NAME OF RESPONSIBLE PERSON
a. REPORT **unclassified**	b. ABSTRACT **unclassified**	c. THIS PAGE **unclassified**	**Same as Report (SAR)**	**12**	

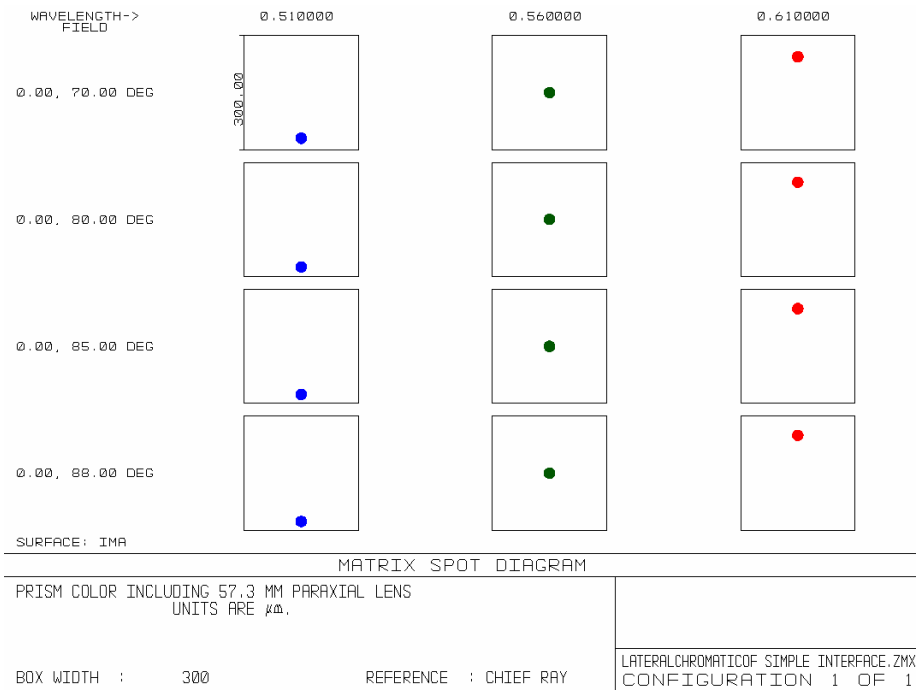

Figure 1. Prism color from transmission through virtual prism of seawater of light from near the air horizon. The image is upside down.

Much higher dispersions than the crown-like[6] dispersion of seawater exist in flint glasses, so a corrective dispersion is attainable without coming close to total internal reflection. In other words, a corrective window consisting of an oppositely-oriented prism can easily be designed and will work under a wide variety of surface tilts. Such a window is designed in Fig. 2. It uses a high-dispersion dense-flint glass, Schott SF11[7], for the negative prism, but could use any one of a number of high-dispersion glasses, including the modern eco-friendly glasses that have superseded many high-lead materials such as SF11.

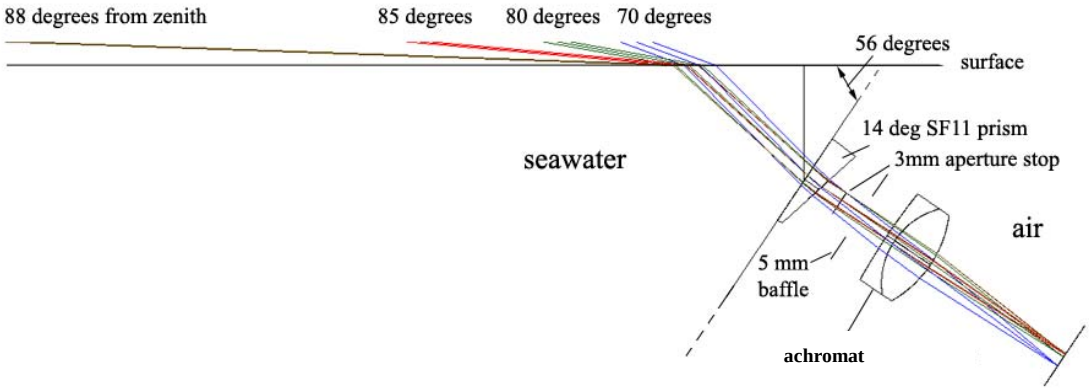

Figure 3. The optical layout of a color-correcting lens design

The virtual seawater-prism angle has shifted from 48 to 56 degrees because the beam is slightly deflected by the prism combination and the horizon must be placed in the field-of-view. The calculated prism angle is 13.4 degrees to correct the water wedge precisely. To increase the number of mounting options, however, this prism was specified at 14 degrees. The lens is a simple achromatic Landscape [8] design of 20-mm focal length, hand-built for this camera because commercially-available pinhole lenses had insufficient focal-plane coverage. The ZEMAX spot diagram of this layout is depicted in Fig. 4. It is corrected for the horizon angle, but operates acceptably well at a zenithal angle of 70 degrees.

Figure 5 is a test image of this situation. The mounted prism was difficult to remove and replace, so an image was taken with the SF11 prism mounted on the camera, but the camera lifted out of the water. Perforations in a backlit mask are stretched into short spectra which are rendered in the left frame as small apostrophes in this monochrome camera. This simulates the inverted

effect of the water with no SF11 prism. Red is highest and strongest because of the low color temperature of the illumination lamp. After the camera is immersed, a new image is then gathered, which is stretched to show about same shape (more on this in the section on distortion below). The air angle of the target is about 15 degrees from the horizon. The image is considerable improved, although it is still a trifle overcorrected because of the finite horizon angle and the slightly-too-large specification of the 14-degree prism angle.

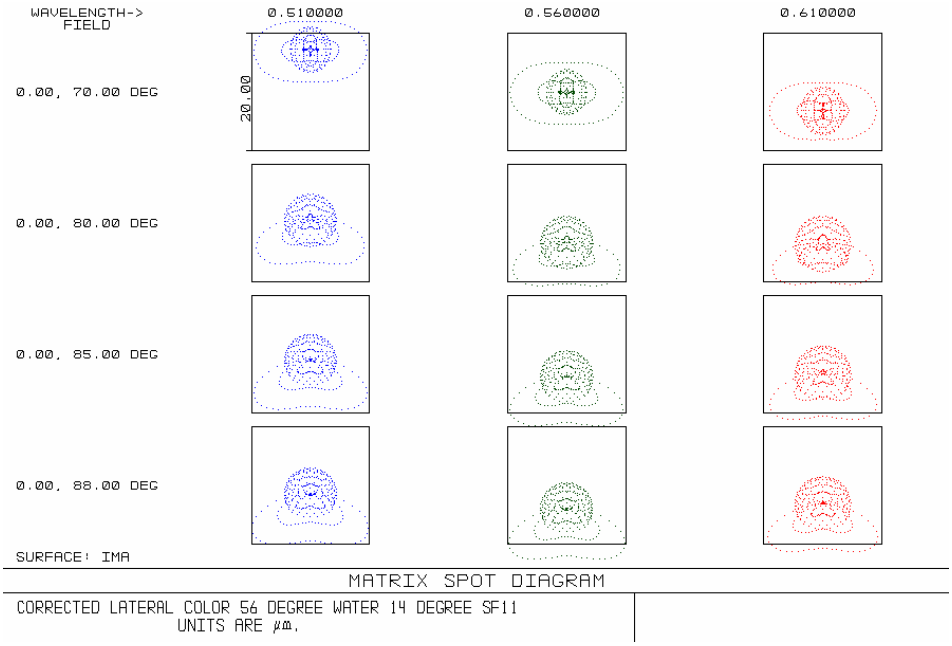

Figure 4. The wedge-spectrum correction with the extra SF11 prism in place. Box is about 2 pixels across.

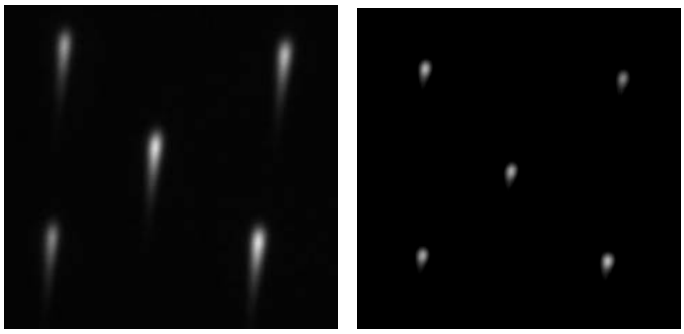

Figure 5. Left: Test of prism in air. Right: Test of prism looking from water into the air.

B. Distortion Near the Horizon

Much of the literature already mentioned has discussed the severe vertical distortion that occurs along the Snell cone. Figure 6 is a depiction of a wide field view taken along the Snell cone, with circles and lines superimposed upon it to guide the eye. The Snell cone is along the *horizon line*. Two *perspective lines* are drawn radially from the zenith. Above the horizon line appears transmitted light from above the water. Below the horizon line is reflected light and the base of the aquarium. In the inset is a detail (taken from another picture, but a similar one) of the near-horizon view. This time the horizon line has not been drawn. The squares occupy about 3.3 degrees at this distance, and the second line up is marked as 6.6 degrees. Below the 3.3 degree line the horizon is inferred but not seen. This image was gathered when there was no chromatic correction, so the horizon is blurred. Clearly, the distortion that occurs at even relatively high angles is severe. From taking the derivative of Snell's formula, one can derive an expression for the vertical magnification:

$$M(\theta) = \left(\frac{n_{air}}{n_{water}}\right) \frac{\sqrt{1-\cos^2(\theta)}}{\sqrt{1-\left(\frac{n_{air}}{n_{water}}\right)^2 \cos^2(\theta)}} \tag{2}$$

where n refers to the respective index of refraction in the respective medium, θ is the horizon angle, and M is the unnormalized magnification (to normalize it to the zenith value, just multiply it by (n_{water}/n_{air}). This normalized magnification is plotted in Fig. 7, and it shows the severe compression that occurs as images approach the horizon. At a little less than 2 degrees, for example, the flattening is 20 to 1.

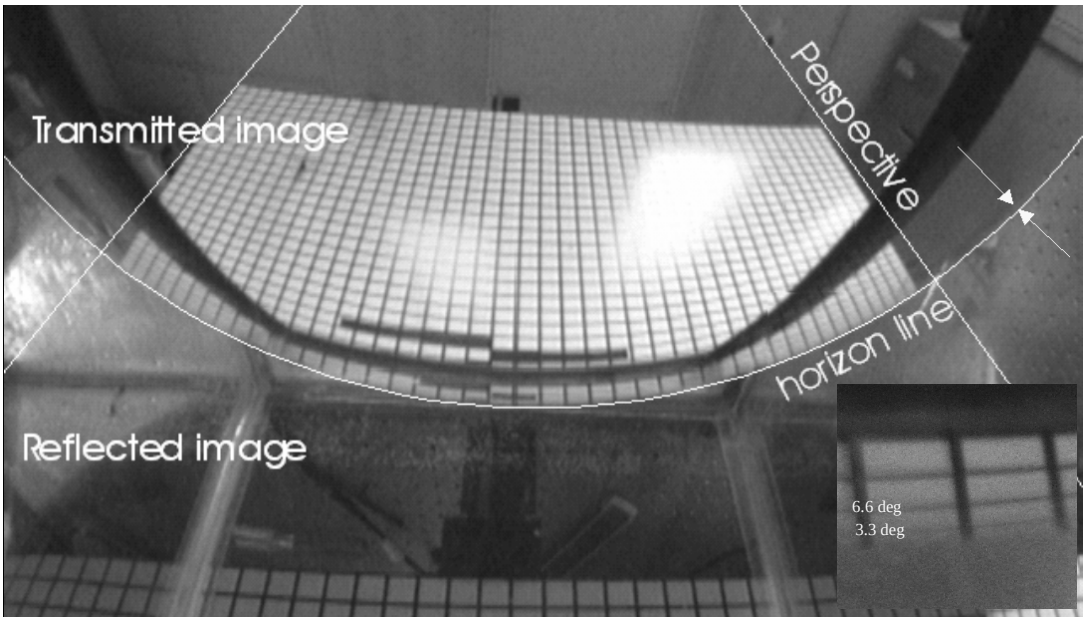

Figure 6. The calm-water aquarium image of the Snell cone (denoted by "horizon line").

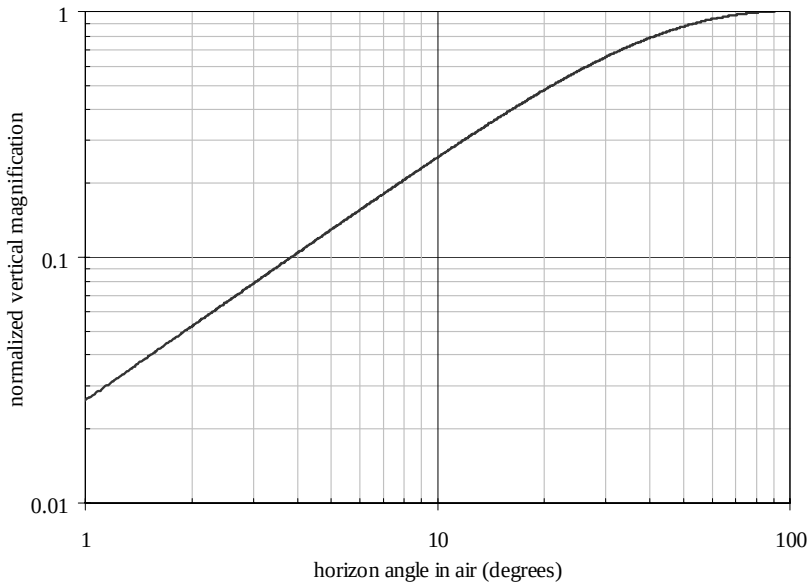

Figure 7. The vertical magnification decreases as the air horizon is approached until the image is compressed into a horizontal line. At 80 degrees from the zenith (10 degrees from the horizon), the normalized vertical magnification is only about a fourth of the horizontal magnification.

Thus, for most useful imaging, it is necessary to take advantage of the natural disturbance of the water's surface to occasionally tilt up the section of surface that the optical system views through so that locally the horizon appears elevated. If the water surface tilts toward the direction of view even 10 degrees (and the next wave does not block the field-of-view), the flattening lessens to 4-to-1 and the image may be discerned. Using resampling, the image is stretched to a rough semblance of the air view, but there is an associated resolution problem. Resampling cannot create information, just interpolate it. Such images have a resampling-induced blurring in the vertical axis. They can be quite sharp horizontally, but the stretching creates a vertical blur. In Fig. 8, even such narrow horizontal detail as the gap between the truck's front fender and the door are visible. Vertical details, however, such as the top of the truck bed, show only the jaggedness from excessive resampling.

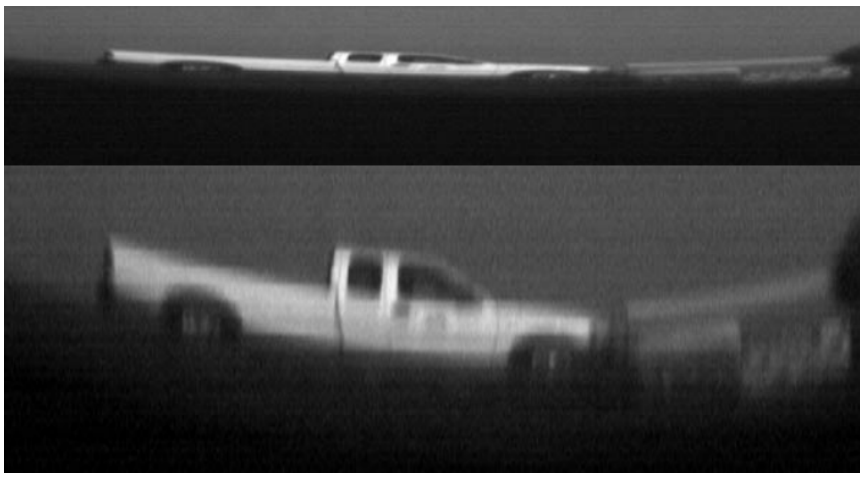

Figure 8. A truck passes a calm pond at a horizon angle of 10 degrees. Picture taken from a few cm below the surface.

The solution is to not sample an image unless it is less compressed. This can be done by waiting until the surface is tilted even more, of course, but that is not a very good solution. The more tilted a surface becomes the greater amount of other deformations that are less advantageous. Another possibility is to increase the focal length of the lens, but using too high a power results in the field-of-view being outside the limits of the frame much of the time. It also increases the number of cameras needed to view in every direction, if the azimuthal angle of the target is not known.

Another design might be to form a near plane-parallel window by tilting the window of the camera by the same amount, say 10 degrees (not shown). Then, whenever the sea surface is tilted by 10 degrees, the window of the camera makes a plane-parallel exit window. This method, however, when extended to anything like a significant field-of-view, takes enormous windows to allow a camera to view the base of the window in a glancing, sidelong, manner. It is not a workable solution.

The only reasonably compact design is to make an anamorphotic lens, also called an "anamorphic" lens. Now these can be constructed either on the Chrétien pattern[9], basically using cylindrical or toroidal lenses to make what amounts to a Galilean telescope in one axis, or on the prism anamorphoser principle, often used in stretching or compressing laser beams in one axis. The prism combinations tend to be bulky and thick, and unlike its use in lasers, this prism anamorphoser must be achromatic.

An impediment may be converted to an advantage in our case by noting that we already have the first element of the anamorphic prism-pair in the seawater wedge. Thus we need only add one more prism to achieve stretching. Such a design is shown in the Fig. 9 ZEMAX layout. It is a two-prism design, but only one prism need be built and carried within the camera, with the forward prism being the wedge of seawater outside the camera and the second prism being carried in front of the iris.

The pair of prisms, one virtual and outside the device, and the other inside the device, are collectively achromatic in the same sense as the previous design. They expand the vertical axis only by a factor of about 1.35 in this experimental instrument, but the ratio could be adjusted by changing the angles and materials of Fig. 9. The primary limit to increasing the magnification of prism anamorphosers is that the final exit angle on the last prism limits the vertical field-of-view, and the greater the stretch, the more limited that field-of-view is.

This anamorphoser was built for an experimental laboratory camera and tested. The two pictures of Fig. 10 were taken in the afternoon and morning, which accounts for the different shadows. The upper one has the anamorphic prism fitted, and each was taken during calm conditions. They depict a door and shuttered window at the end of a floating pier. The entrance pupil of the camera is a few inches below the surface of the water, and these images were only mildly compressed at a horizon angle of about 20 degrees. The door spring-dashpot and the railing are pointed out, and at least in these two images, the anamorphic system leads to image improvement.

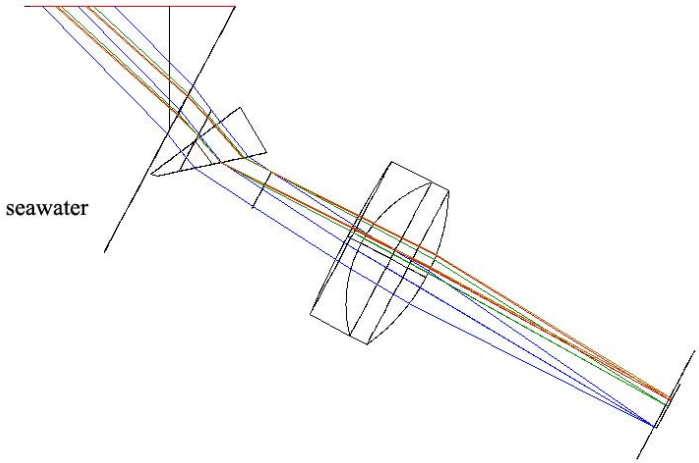

Figure. 9. Experimental anamorphic design. The small prism is Schott N-F2

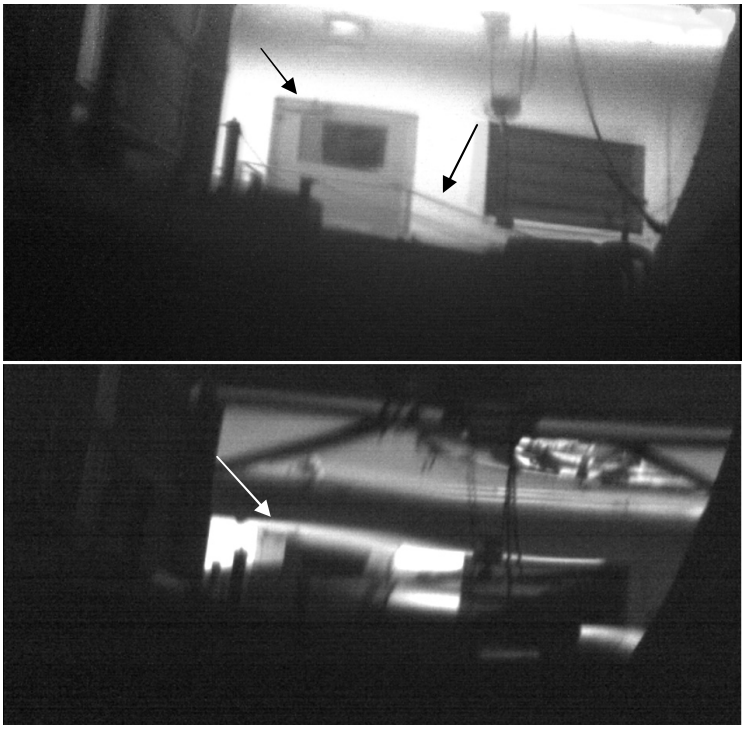

Figure 10. Results of the experimental anamorphotic configuration.

C. Blurring from Refraction

Clearly, the optical difficulties in sections A and B are important, but they are straightforwardly solved. The difficulty that creates the greatest problem is optical refraction at the interface between the two media. The surface of the water is distorted by a spectrum of waves extending from long gravity waves to short capillary waves. This structural distortion is translated into optical aberrations on the bundle of light entering the entrance pupil of the lens. If the pupil is extended up along the parallel ray bundle it intercepts the strongly refracting surface in a small oval shape. If the pupil is large, there is much structure on this surface. If the pupil is small, there is less structure. Thus, small pupils have a greater probability of being simple windows.

By diminishing the size of the pupil further, a condition will be reached where the only remaining structure is the tilt given the wave front by the refraction. Yet still the scene is not visible for a highly structured surface. Only for relatively smooth surfaces is an image discerned. (The exposure is assumed fast enough to render motion negligible.)

The cause is anisoplanatism, or formally the lack of space invariance in the impulse response of an optical system [10]. Anisoplanatism is simply the lack of correlation of the pupil aberration from one look angle to another. As the pupil is drawn up to the refracting surface, a single wave front shape on that pupil influences the whole field-of-view but any significant separation

results in the situation of *a* (these situations are sketched for a vertical field-of-view in Fig. 11). Thus, optimum conditions prevail when the pupil is close the surface, although this is a seldom-realized condition for any outdoor, real-world water surface. Indeed, it is only for calm water that isoplanatism can be precisely achieved at all. Most commercial camera lenses, which contain the virtual position of the entrance pupil far behind the front surface of the lens, also preclude this form of isoplanatism. Keeping the pupil as near as possible to the surface and keeping the prisms small were the reasons behind using the stop-forward lens designs presented earlier in this paper.

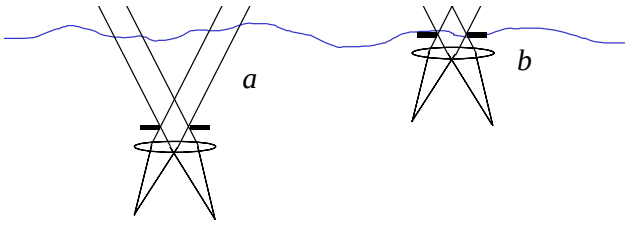

Figure 11. *a*) Anisoplanatism caused by different refracting regions on the surface. *b*) Isoplanatism is recovered when the pupil is at the surface.

Anisoplanatism has been discussed in depth for atmospheric propagation by Fried [11], chiefly having to do with astronomical adaptive optics. Fried and others have also discussed "lucky" imaging, or constructing a composite image from a carefully selected subset of images [12][13], In Snell-cone optics, lucky imaging takes on a new form. It is not merely waiting for the view to clear, but waiting for the view to be possible. Fig. 12 shows the problem with viewing near the horizon. The obscured or total-internally-reflected cases are a significant fraction of the possibilities, depending on the viewing angle and the deformation of the surface, of course. In this experiment, lucky image sorting was done.

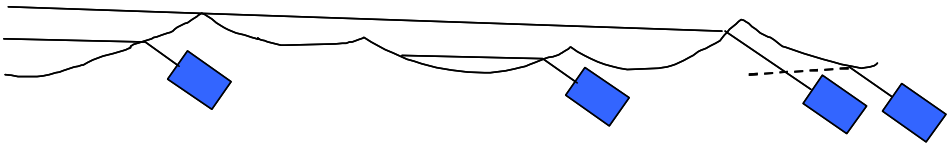

Figure 12. Horizon views must be sorted from a sequence of images.

A patch of the image that is isoplanatic is not the only condition that is required for successful imaging. The wave front emerging from the entrance pupil must be fairly flat before good imaging is possible. If it is not (see Fig. 11 *b*), the image may be approximately isoplanatic but still not sharp. In the lucky exposures method, if the wave front is accidentally flat or very slightly curved over at least a part of the image, it necessarily has a large isoplanatism patch. If it not occluded as some of the examples are in Fig. 12, we will see it.

We can expand the wave front on the generalized pupil by a set of complete orthogonal polynomials, where one form of the low orders is presented in Table 1 [14]; ρ is the normalized radius of the pupil and φ is an arbitrary azimuth angle in the plane of the pupil. These terms are associated with a set of coefficients, and if taken to infinite order in ρ, completely describe the wave front. In practice, the coefficients diminish for higher powers of ρ.

This orthogonal set was first defined on the unit circle by Frits Zernike, who called them circle polynomials. Note that the lowest orders, namely piston and distortion, are still flat and hence will not blur the image (piston is mostly a computational device). The lowest-order blurring aberrations are defocus and the two axes of astigmatism. If the pupil is kept small enough, we can approximate this expansion by its first six terms, truncating the series at Z_6.

TABLE I
AN ORTHOGONAL DESCRIPTION OF ABERRATIONS INDUCED ON AN ENTRANCE PUPIL.

Term	*Zernike polynomial*	*Name*
Z_1	1	piston
Z_2	$2\rho\cos(\varphi)$	x-distortion
Z_3	$2\rho\sin(\varphi)$	y-distortion
Z_4	$\sqrt{3}(2\rho^2-1)$	defocus
Z_5	$\sqrt{6}\rho^2\sin(2\varphi)$	45-135 deg astigmatism
Z_6	$\sqrt{6}\rho^2\cos(2\varphi)$	0-90 deg astigmatism
Z_7	$\sqrt{8}(3\rho^2-2)\rho\sin(\varphi)$	y-coma (drumhead)
Z_8	$\sqrt{8}(3\rho^2-2)\rho\cos(\varphi)$	x-coma (drumhead)
Z_9	$\sqrt{8}\rho^3\sin(3\varphi)$	30-150 deg trefoil
Z_{10}	$\sqrt{8}\rho^3\cos(3\varphi)$	0-120 deg trefoil
Z_{11}	$\sqrt{5}(6\rho^4-6\rho^2+1)$	spherical aberration
...	...	...

Note that both defocus and astigmatism terms are proportional to ρ^2, meaning that in one or two dimensions, they follow the first term in the expansion of a spherical deformation. Given the lens focal length (20 mm) and the aperture dimension (2.8 mm), the blurring or stretching at the focal plane may be readily calculated as the values in Table II. As long as the radius of the sea surface is beyond 0.5 m, then the destructive effects of sea curvature is relatively small, but it quickly becomes severe at small radius. It was witnessed during the test that when a capillary wave-train went over the camera, little was visible. The probable reason was that the radius of curvature was too small, and hence the induced blurring was too great.

One may also use the sum of the three circle polynomials Z_4 through Z_6 as a kernel for a deconvolution algorithm, searching over a three-dimensional coefficient space for the best fit to a sharpness metric such as an edge finder or entropy algorithm.

TABLE II
BLURRING IN MICROMETERS DUE TO A SEAWATER SURFACE OF RADIUS R

R(mm)	blur(μm)	pixels
100	191	18.0
200	95	9.0
300	64	6.0
400	48	4.5
500	38	3.6
600	32	3.0
700	27	2.6
800	24	2.2
900	21	2.0
1000	19	1.8

III. ACTUAL IMAGES

A. The Camera

The camera is a PhotonFocus Hurricane™ high dynamic-range linear-log CMOS type. It is important for this application that the camera be a global-shutter type and that it not have any progressive scan or interline artifacts. It is capable of extremely fast exposures (less than 0.1 ms) and because the pixels are 10.6 by 10.6 μm, has reasonable sensitivity. It renders the image in 4096 levels.

B. The Test Bed

The test bed (Fig. 13) is a 3-channel unit that uses the achromatic wedge but not the anamorphoser. The anamorphic attachment was viewed as too risky at the time this unit was designed. It is connected to shore computers by a fiber-optic cable and a power-carrying copper wire. It was not buoyed naturally, but attached between pilings.

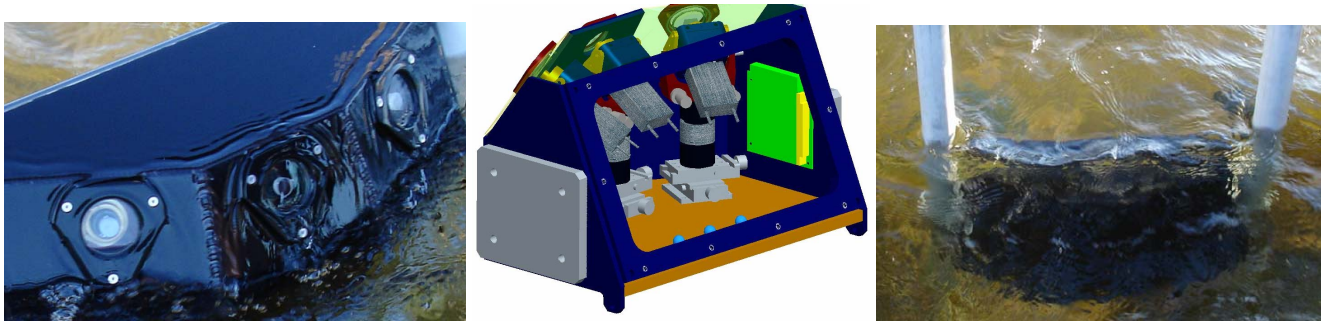

Figure 13. The Areté 3-channel test-bed unit.

C. The Site

The site was an abandoned campground on Choctawhatchee Bay at Hammock Point. Hurricanes have ruined its pier and there are pilings standing about with separations of 1.5 to 3 m. There is about 6 km of open bay in front of the test side. Wind was between 6 and 12 kn. There was no surf action.

D. The Targets

The targets were various vehicles, resolution targets, and targets of opportunity ranging from 0 degrees to about 5 degrees off the horizon. They are shown in later pictures.

IV. DISCUSSION

The small amount of data that we have been able to analyze thus far have taught us that this is a problem of sorting through massive amounts of information for those tiny snippets of image which contain enough detail to be profitably processed.

The lucky imaging approach takes advantage of the fact that the undulating water surface occasionally provides a surprisingly sharp view of the scene—perhaps once in hundreds of frames. Finding the lucky frame can be a time consuming process, so software is needed to automatically select the useful frames from very large data sets. An image processing graphical user interface was created that allows easy visualization of the data and contains a sorting algorithm to score the image quality. Fig. 14 is a sequence of images that occurred over only 0.2 s. The scene oscillated between bad and good in times less than the frame rate of 20 Hz.

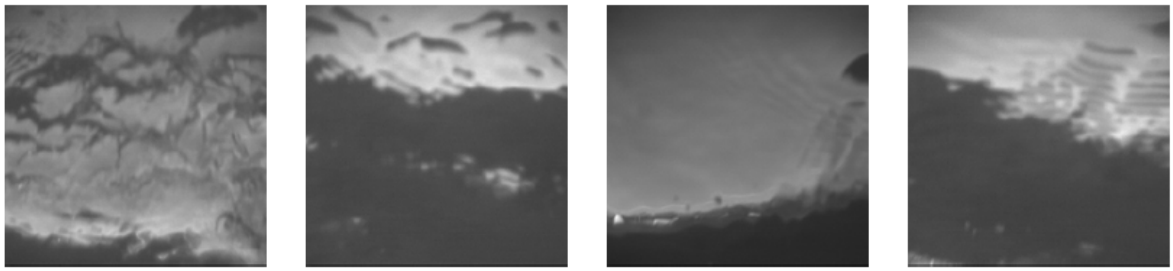

Figure 14. Four consecutive frames. Only the third is reasonably interesting.

In the course of analyzing data collected under a variety of conditions, it has become obvious that it is very difficult to design a sorting metric that will be effective in every circumstance. The first sorting metric was developed using data collected in a pond with an earlier version of the sensor. The water was very calm so the images were fairly stable and underwent relatively modest fluctuations in sharpness. In some sense, all pond images are lucky frames since they all contained more or less recognizable objects. The initial step of the developed metric is processing the images with a Sobel filter and calculating the cumulative distribution function (CDF) of the filtered images. The image score was calculated as the value of the CDF at a fixed level of the filtered images. This metric succeeded in finding the sharpest images even under quite varied scenery, but depended on having a relatively stable scene with which to work, i.e. calm water, and also depended on high contrast targets.

A. The Bay Sort Metric

Sorting the Chocktawhatchee Bay data is considerably more challenging due to the increased wave content in the imagery. This increase lead to a development of a new sorting algorithm. The improved sorting algorithm is initiated by finding subregions of the image that are likely to contain sharp boundaries between light and dark patches of water. This is accomplished by calculating brightness histograms of the image subregions, like those shown in Fig. 15, and looking for indications of a multimodal distribution and higher than average variance. Subregions are flagged as “interesting” based upon a complex formula involving the properties of the histograms’ variance and the number of distinct peaks. The final sort metric is calculated based upon the difference between the number of adjacent “interesting” subregions forming the longest row and the number of distinct connected “interesting” subregions. This sort metric tends to favor images with a distinct, elongated horizon and reject images with “interesting” subregions randomly scattered across the image, namely the basket pattern of capillary waves. (See Fig. 16.)

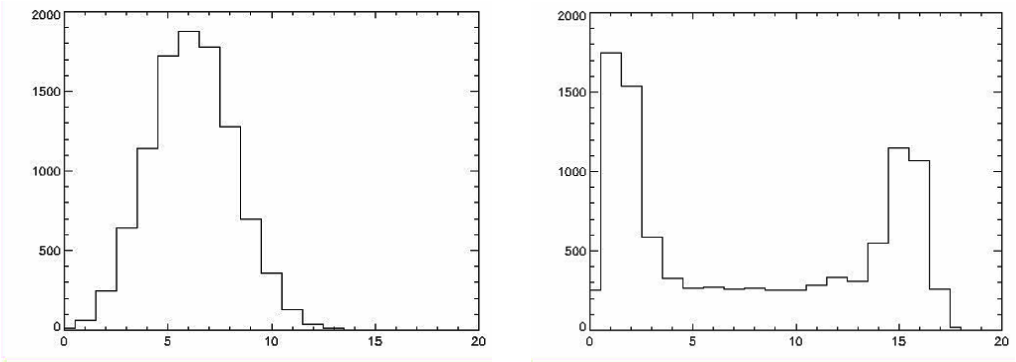

Figure 15. Two histograms: (left) “uninteresting,” and (right) “interesting.”

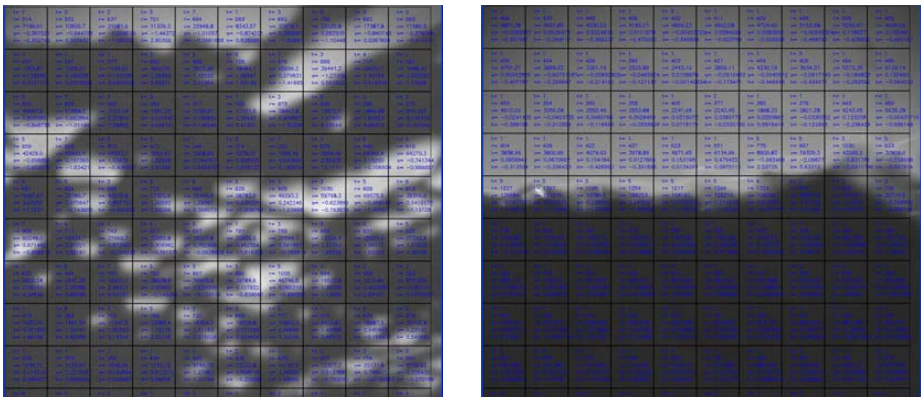

Figure 16. (Left) Uninteresting frame vs. (Right) Interesting frame.

The effectiveness of the sorting metric was assessed by counting the number of lucky frames in a variety of datasets and determining the number of lucky frames found near the top of the sorted list. A subjective judgment was necessary to determine which frames were considered lucky, and owing to the tedium of hand-selecting lucky frames, only a few subsets of the image sequences were analyzed.

Table III summarizes the results of this analysis. Two datasets from the bay test were analyzed, one with 5-inch waves and the other with 6-inch waves (peak-to-peak amplitude). The number of lucky frames was tabulated in three subsets of the imagery: the first 20% of the frames, a set of 1000 contiguous frames drawn from the 3rd quartile, and the last 1000 frames. The images were ordered both chronologically and according to the ranking assigned by our sort metric.

Analyzing the 8400 chronologically ordered frames in the 5-inch wave dataset yielded a total of 57 lucky frames. Assuming the lucky frames are more-or-less evenly distributed chronologically, the 5-inch data set therefore contains approximately 220 lucky frames out of 32000, about a 0.7% lucky frame rate. When the sorting metric is applied, a total of 229 lucky frames are found in the top 20%, a number consistent with the estimated total number of lucky frames, and none are found in the other sorted data subsets. This verifies that the sort metric successfully moved the bulk of the lucky frames to the front.

In the 6-inch dataset, a total of 13 lucky frames were found in a total of 5400 chronologically ordered frames. This leads to an estimate that about 40 lucky frames are present in the entire 17000-frame dataset, about a 0.2% lucky-frame rate. In the sorted frames a total of 20 lucky frames occurred in the top 20% and none in the other two subsets. The estimate for the total number of lucky frames suggests there may be more found below the top 20%, but once again the sort metric performed well in selecting lucky frames. Based upon the pond data and the two bay test datasets, a trend emerged that show lucky frames become increasingly rare with higher amplitude waves.

The sort metric designed using Chocktawhatchee Bay test data was applied to the pool test data taken during the camera checkout, which is considerably different because the pool has many more high elevation objects (trees, house, targets, etc.), and did not perform well. This shows that it is extremely challenging if not impossible to design a single sort algorithm that will select lucky frames under all circumstances, but the metric designed for the Bay test data should work well whenever the objects in the scene are confined to low elevations. A secondary sort metric can be developed and applied to the higher elevation target allowing one tool to work in both instances depending upon the task at hand.

The Chocktawhatchee Bay data are notable for their lack of surf action. An experiment in the presence of surf is suggested, since it regularly lifts the surface toward the shore, and necessarily has a long wavelength.

TABLE III
ANALYSIS OF SORTING METRIC

Total number of frames	32000		17000	
Estimated lucky frame fraction	0.7%		0.2%	
	Sorted	Chronological	Sorted	Chronological
Number of lucky frames in top 20%	229 / 6400	9 / 6400	20 / 3400	7 / 3400
Number of lucky frames in contiguous 1000 frames in 3rd quartile	0 / 1000	8 / 1000	0 / 1000	1 / 1000
Number of lucky frames in last 1000	0 / 1000	40 / 1000	0 / 1000	5 / 1000

B. Sub-regions

There is reason to hope that sub-regions of the image can be collected to form larger images. In Fig. 17, we see how individual regions can show clarity even if the rest of the image is blurred beyond recognition. In *a*) we see the in-air field-of-view, except that the leftward piling is a little far to the left and no crossing rope is visible to the water camera. Frame *b*) shows that if one is very patient, one can see a recognizable scene clear across the frame. This is, in fact, the field of two cameras stitched together to show the building at the right. By subdividing the frame to sub-regions, we can perhaps make a frame out of pieces. There is one troubling disadvantage with this procedure, however, and that is the seemingly random position that resolved areas end up. That is

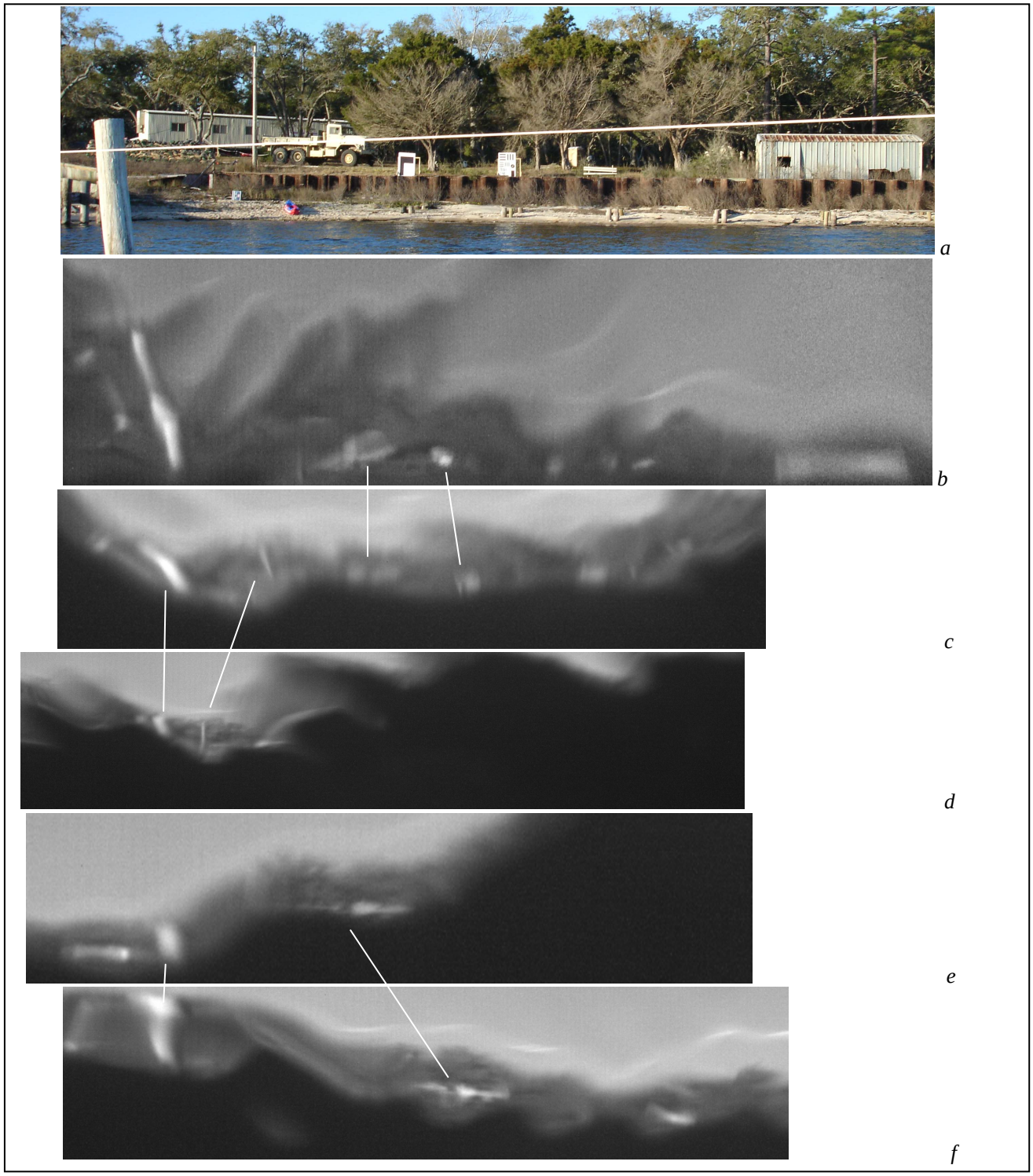

Figure 17. Image frames occasionally show glimpses through the blur regions, but only in small gaps.

indicated by the connections indicated to obviously the same items in the separate fields-of-view. The left-right position of these resolved areas of the target are only approximately the same from frame to frame. This makes sense if we consider that the values of the non-blurring Zernike tilt coefficients of Z_2 and Z_3 vary quite a bit even for these fairly uniform surfaces.

C. More Work for Different Environments

The success or lack of it of the Chocktawhatchee Bay test perhaps depended on the direction (it came from the rear quarter compared to the look angle) and uniformity of the wind, and also the presence of the support pilings as generators of air turbulence. In an early St. Andrews Bay test of a laboratory camera, other performance values were witnessed. The laboratory camera was held relatively far from its supports, and hence did not have a nearby source of capillary waves, in the snippet of imagery represented by the frames in Fig. 18, the rate of interesting frames was at least 1 in 50. Clearly more work is needed in different environments before deciding that lucky imaging produces too low a frame rate.

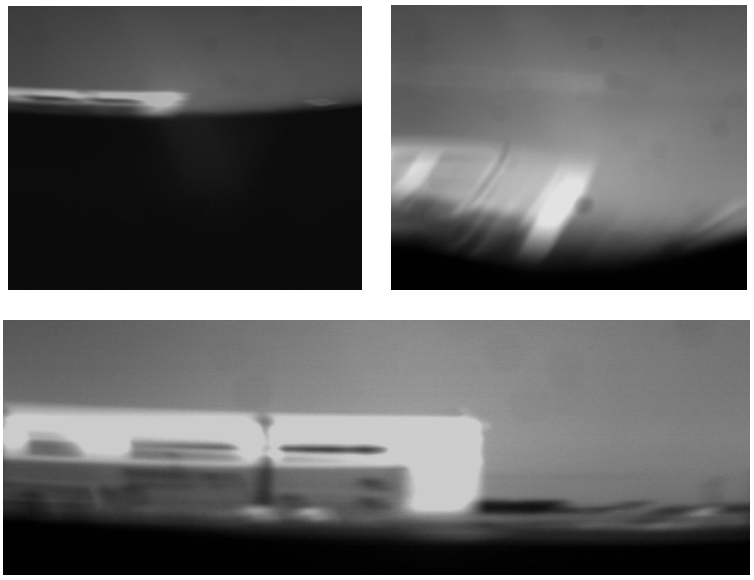

Figure 18. Frames gathered under different conditions. The bottom of the lower frame is less than 1 degree high.

V. CONCLUSIONS

1) The likeliest method of near-horizon viewing is to use a small entrance pupil and to place it as near to the surface as possible.
2) Correction of wedge prism color is necessary in near-horizon air-to-water viewing. Owing to the crown-like nature of seawater dispersion, this correction is easy, requiring no more than a thin dispersive prism.
3) The distortion that occurs when light is coming from the horizon may be mitigated by waiting for a surface deformation that leans toward the viewed horizon. It may be further lessened by using anamorphotic lenses.
4) The method of lucky imaging may be used to construct a horizon image. This process is extremely inefficient, however, which leads to suggested further work on methods to speed it up, as well as investigations in other environments.

REFERENCES

[1] Hubert Biezeveld, *et al*., "Analysis of Pictures Taken with an Underwater Camera," *The Physics Teacher*, vol. 43, no. 3, pp. 158-160, March 2005.
[2] Jearl Walker, "What is the fish's view of the fisherman and the fly he has cast on the water?" *Sci. Am.*, vol. 250, no. 3 pp. 108-113. 1984.
[3] András Barta and Gábor Horvath, "Underwater binocular imaging of aerial objects versus the position of eye relative to the flat water surface," *J. Opt. Soc. Am. A*, vol. 20, pp. 2370-2377, December 2003.
[4] Bruce H. Walker, *Optical Design for Visual Systems*, p. 5, SPIE Press, 2000.
[5] ZEMAX Development Corp. *ZEMAX-EE Optical Design Program*, May 15, 2007.
[6] Joseph M. Geary, *Introduction to Lens Design, With Practical ZEMAX® examples*, p. 55, Willmann-Bell, Inc. 2002.
[7] Schott North America, Inc., 400 York Avenue, Duryea, PA 18642.
[8] Geary , *op. cit.*, p. 217 *et seq*.
[9] H. Chrétien, "Anamorphotic Lens System and Method of Making the Same," *U.S. Patent no.1,962,892*, June 12, 1934.
[10] Joseph W. Goodman, *Introduction to Fourier Optics*, p. 19, McGraw-Hill, 1968.
[11] David L. Fried, "Anisoplanatism in adaptive optics," *J. Opt. Soc. Am.*, vol. 72, no. 1, pp. 52-61, January 1982.
[12] David L. Fried, "Probability of getting a lucky short-exposure image through turbulence," *J. Opt. Soc. Am*., vol. 68, no. 12, December 1978.
[13] N.M. Law, C.D. Mackay, and J.E. Baldwin, "Lucky Imaging: High Angular Resolution Imaging in the Visible from the Ground," *Astronomy & Astrophysics*, vol. 446, no. 2, pp. 739-745, February 2006.
[14] Robert J. Noll, "Zernike polynomials and atmospheric turbulence," *J. Opt. Soc. Am*., vol. 66, pp. 207-211, 1976.